Adaptive Dead-Time Compensation Strategy for Permanent Magnet Synchronous Motor Drive

Naomitsu Urasaki, *Member, IEEE*, Tomonobu Senjyu, *Senior Member, IEEE*, Katsumi Uezato, and Toshihisa Funabashi, *Senior Member, IEEE*

***Abstract*—This paper presents an adaptive dead-time compensation strategy to obtain fundamental phase voltage for inverter-fed vector-controlled permanent magnet synchronous motor drives. A phase dead-time compensation voltage (DTCV) to compensate the disturbance voltage due to undesirable characteristics of inverter, such as dead time, turn on/off time of switching devices, and on-voltages of switching devices and diode, is transformed into q-axis DTCV in the rotor reference frame. The relationship between q-axis DTCV and a dead-time compensation time (DTCT) is investigated. DTCT is identified online by using q-axis disturbance voltage, which is estimated by a disturbance observer. The amplitude of phase DTCV is adaptively determined according to the identified DTCT. The accuracy of identified DTCT is experimentally confirmed by calculating the mean absolute percentage error (MAPE) between calculated active power and measured one. MAPE for adaptive DTCT is within 5% at any operating point and is less than that for the fixed DTCT.**

***Index Terms*—Dead-time compensation time (DTCT), dead time compensation voltage (DTCV), disturbance voltage, permanent magnet synchronous motor (PMSM), voltage source inverter.**

I. Introduction

VOLTAGE source inverter fed permanent magnet synchronous motor (PMSM) drives have widely been developed for the last decade. Several applications, such as rotor position sensorless drives, need an information of fundamental phase voltage [1], [2]. Since fundamental phase voltage cannot be detected from inverter output terminal, commanded voltage is usually used instead of the actual one. However, commanded voltage never agrees with the actual fundamental phase voltage due to undesirable characteristics of inverter, such as dead time, turn on/off time of switching devices, and on-voltages of switching devices and diodes. Dead time is vital to avoid short-circuit of inverter legs. Turn on/off time and on-voltages inevitably exist in practical devices. To cope with this problem, several authors have made attempt to compensate undesirable characteristics of inverter [3], [4]. In [3], a dead-time compensation voltage (DTCV) was introduced. DTCV is determined from the analytical result of the average error between ideal and actual inverter output voltages taking dead time into account. Although implementation of this method is easy, turn on/off time and on-voltages effects cannot be compensated. In [4], a dead time compensation time (DTCT) was introduced instead of dead time. DTCT equivalently includes turn on/off time and on-voltage components as well as dead time. Thus, this method can compensate not only dead time effect but also turn on/off time and on-voltages effects. Since DTCT is usually an unknown parameter, it is necessary to identify DTCT. In [4], DTCT is identified by a developed adaptive identification process in advance. Then, a fixed DTCT is utilized for dead time compensation strategy. However, the fixed DTCT is not always valid because DTCT varies with operating point [5].

To overcome this problem, an adaptive dead time compensation strategy using disturbance observer for PMSM drive has been proposed [6]. In this method, $d-q$ axes DTCVs in the rotor reference frame are estimated online using the disturbance observer which is developed based on mathematical model of PMSM. Then, estimated $d-q$ axes DTCVs are added to the $d-q$ axes commanded voltages generated with current controller directly. Since fundamental frequency of d-q axes DTCV is six times of driving frequency, estimation delay occurs with increase in driving frequency. The estimation delay results in degradation of dead time compensation.

This paper presents an adaptive dead-time compensation strategy for inverter-fed vector-controlled PMSM drive. The relationship between DTCT and q-axis DTCV, when d-axis current is zero, is investigated. In this paper, it is assumed that q-axis DTCV is identical to the q-axis disturbance voltage due to undesirable characteristics of the inverter. The q-axis disturbance voltage is estimated by a disturbance observer. DTCT is calculated online using estimated q-axis disturbance voltage. An adaptive DTCT is utilized for deciding the amplitude of phase DTCV. The proposed method has an advantage that it is lightly affected to the estimation delay of disturbance observer because only the amplitude of phase DTCV is adjusted. In addition, only the q-axis disturbance observer is required for the adaptive dead time compensation strategy. Simulation and experimental results confirm the usefulness and validity of the proposed method.

II. PMSM Drive System

A. Definition of Coordinate Axes

Fig. 1 shows definition of coordinate axes. The a-b-c axes are defined as the flux orientation of each phase current. The d-axis is defined as the permanent magnet flux orientation. The q-axis is defined as the advanced direction by 90° from d-axis. The d-q axes are synchronized with the rotor of PMSM.

Manuscript received September 9, 2003; revised March 17, 2004. Paper no. TEC-00236-2003.

T. Funabashi is with the Power System Engineering Division, Meidensha Corporation, Tokyo 103-8515, Japan (e-mail: funabashi-t@mb.meidensha.co.jp).

N. Urasaki, T. Senjyu, and K. Uezato are with the Department of Electrical and Electronics Engineering, University of the Ryukyus, Okinawa 903-0213, Japan (e-mail: urasaki@tec.u-ryukyu.ac.jp; b985242@tec.u-ryukyu.ac.jp; uezato@eee.u-ryukyu.ac.jp).

Digital Object Identifier 10.1109/TEC.2006.875469

0885-8969/$25.00 © 2006 IEEE

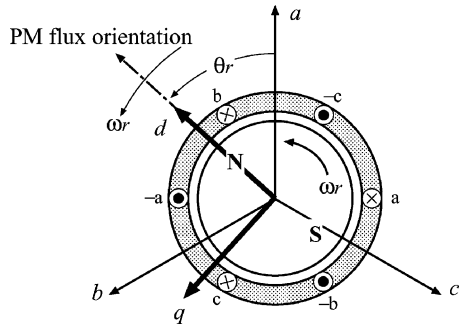

Fig. 1. Definition of coordinate axes.

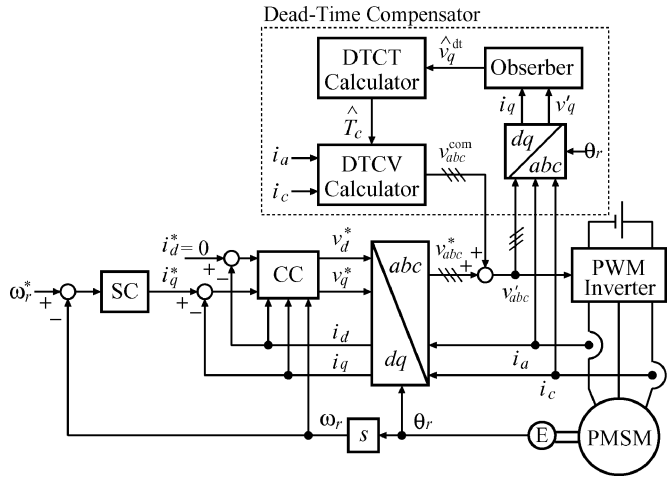

Fig. 2. Vector-controlled PMSM drive system for variable speed drive.

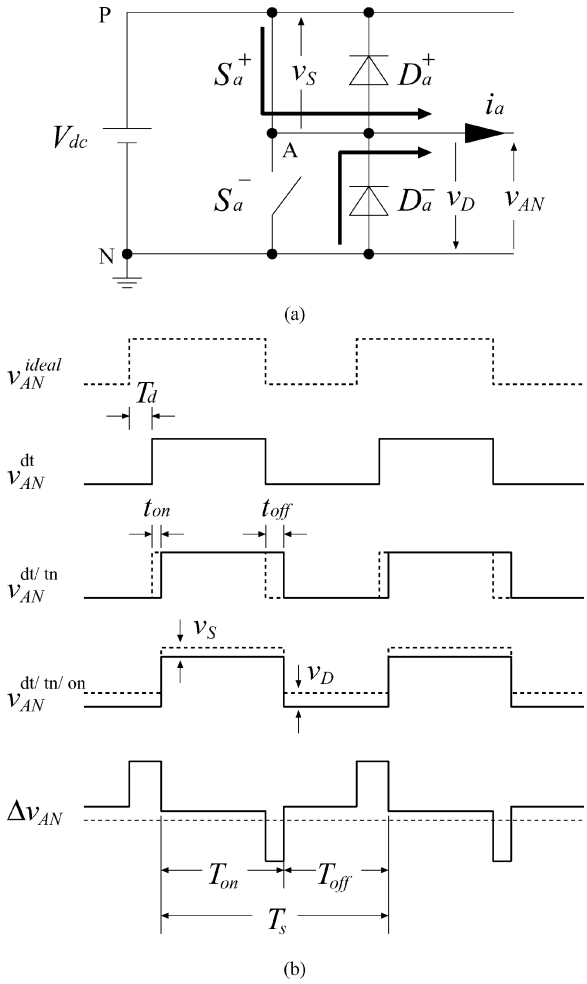

Fig. 3. Relationship between a-phase ideal and actual inverter output voltages for $i_a>0$. (a) Channel flow of a-phase current. (b) a-phase inverter output voltage.

B. System Configuration

Fig. 2 shows typical vector-controlled PMSM drive system. The proposed dead time compensator is indicated by dashed block. The detail of this compensator is discussed in Section IV. Since PMSM obtains excitation from permanent magnet on the rotor, the d-axis current, which is excitation component is set at zero in the typical vector-controlled PMSM drive. In Section III, DTCT when d-axis current is zero is formulated.

III. Dead-Time Compensation

A. Formulation of DTCV

Fig. 3(a) shows the channel flow of a-phase current for positive direction $(i_a>0)$. The a-phase current i_a flows through switching device S_a^+ during on-period $T_{\rm on}$. On other way, it flows through diode D_a^- during both off-period $T_{\rm off}$ and dead time T_d. Thus, a-phase inverter output voltage $v_{\rm AN}$ for dead time period is equal to that for off-period. The relationship between a-phase ideal and actual inverter output voltages for $i_a>0$ is shown in Fig. 3(b). Due to dead time T_d, actual voltage becomes $v_{\rm AN}^{dt}$. In addition, due to turn on time $t_{\rm on}$ and turn off time $t_{\rm off}$ of switching device S_a^+, actual voltage becomes $v_{\rm AN}^{dt/tn}$. Furthermore, due to on-voltages v_S of switching device S_a^+ and v_D of diode D_a^-, actual voltage becomes $v_{\rm AN}^{dt/tn/\rm on}$. As a result, the difference between ideal and actual inverter output voltages becomes $\Delta v_{\rm AN}(=v_{\rm AN}^{\rm ideal}-v_{\rm AN}^{dt/tn/\rm on})$.

Fig. 4(a) shows the channel flow of a-phase current for negative direction $(i_a<0)$. The a-phase current i_a flows through diode D_a^+ during both on-period $T_{\rm on}$ and dead time T_d. On other way, it flows through switching device S_a^- during off-period $T_{\rm off}$. Thus, a-phase inverter output voltage $v_{\rm AN}$ for dead time period is equal to that for on-period. The relationship between a-phase ideal and actual inverter output voltages for $i_a<0$ is shown in Fig. 4(b). From a similar analysis, the difference between ideal and actual inverter output voltages becomes $\Delta v_{\rm AN}(=v_{\rm AN}^{\rm ideal}-v_{\rm AN}^{dt/tn/\rm on})$.

To compensate undesirable characteristics of inverter, a DTCV is added to the commanded voltage generated with current controller in the vector-controlled PMSM drive system. Since DTCV corresponds to an average value of $\Delta v_{\rm AN}$ over switching period $T_{\rm s}$, a-phase DTCV $v_a^{\rm com}$ is derived from the above analytical result as

$$v_a^{\rm com}=\frac{T_c}{T_{\rm s}}V_{\rm dc}{\rm sgn}(i_a) \tag{1}$$

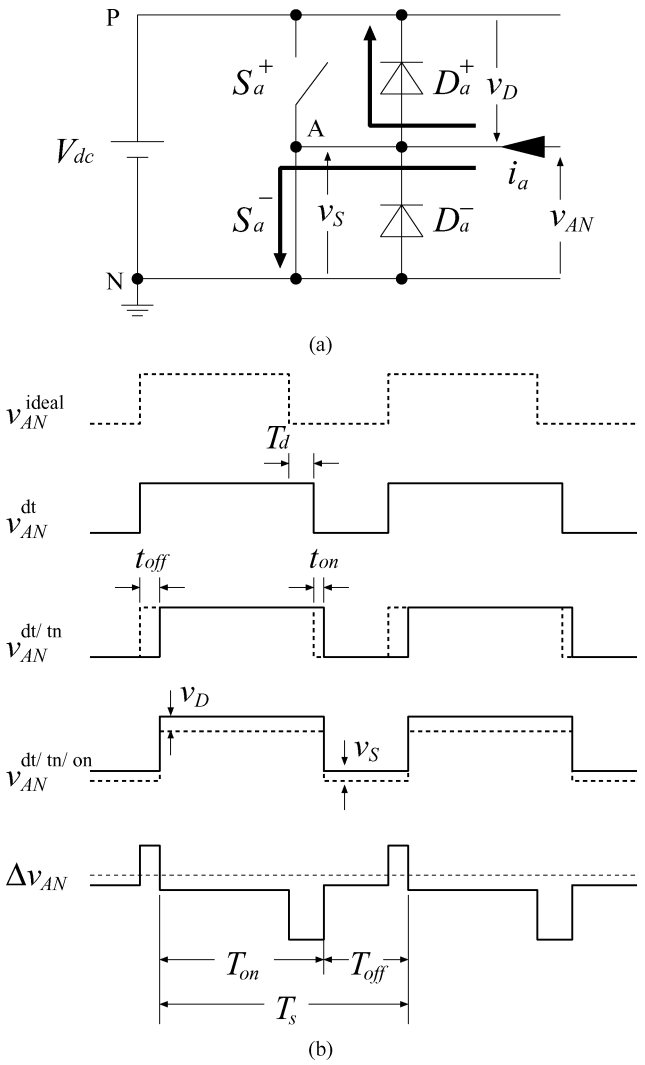

Fig. 4. Relationship between a-phase ideal and actual inverter output voltages for $i_a<0$. (a) Channel flow of a-phase current. (b) a-phase inverter output voltage.

where T_c, T_s, and V_dc are DTCT, switching period, and dc-link voltage, respectively. DTCT is defined as

$$T_c = T_d + t_\mathrm{on} - t_\mathrm{off} + \frac{V_\mathrm{on}}{V_\mathrm{dc}} T_\mathrm{s} \tag{2}$$

where $T_d, t_\mathrm{on}, t_\mathrm{off}$, and V_on are dead time, turn on time, turn off time, and average on-voltage, respectively. The average on-voltage V_on is defined as

$$V_\mathrm{on} = \begin{cases} \frac{T_\mathrm{on}}{T_\mathrm{s}} v_S + \frac{T_\mathrm{off}}{T_\mathrm{s}} v_D & (i_a>0) \\ \frac{T_\mathrm{off}}{T_\mathrm{s}} v_S + \frac{T_\mathrm{on}}{T_\mathrm{s}} v_D & (i_a<0) \end{cases} \tag{3}$$

where v_D, v_S are on-voltages of diodes and switching devices and $T_\mathrm{on}, T_\mathrm{off}$ are on-period and off-period of the upper-arm of inverter leg, respectively. It is noted that both average on-voltages for positive and negative current directions are almost same because on-period T_on for $i_a>0$ is almost identical to off-period T_off for $i_a<0$, and vice versa. Similarly, b-phase and c-phase DTCVs are also derived.

TABLE I
SPECIFICATIONS OF TESTED INVERTER

maximum rated voltage	V_{CE}	600 V
maximum rated current	I_C	30 A
dead-time for IGBT	T_d	5.0 μs
turn-on time of IGBT	t_{on}	0.6 μs
turn-off time of IGBT	t_{off}	2.0 μs
on-voltage of IGBT	v_S	1.9 V
on-voltage of diode	v_D	2.5 V

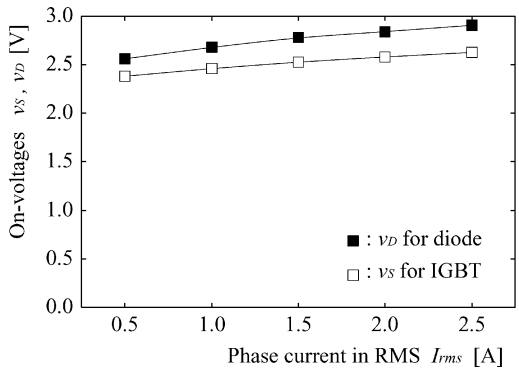

Fig. 5. On-voltages of diodes and IGBT for tested inverter.

B. On-Voltages of Switching Devices and Diodes

Table I shows the specifications of tested inverter. An insulated gate bipolar transistor (IGBT) module is utilized for switching devices. The dead time for IGBT is set at 5 μs.

Fig. 5 shows the on-voltages of diode and IGBT for the root mean square (RMS) value of phase current. These on-voltages are measured by digital oscilloscope TDS3014B. In the tested inverter, measured on-voltage of diode is greater than that of IGBT $(v_D>v_S)$. It can be confirmed that measured on-voltages qualitatively coincide with the specifications irrespective of the RMS value of phase current. On this condition, as can be seen from (3), average on-voltage V_on for $i_a>0$ increases with decreasing rotor speed when the RMS value of phase current is constant, i.e., load condition is maintained, because on-period T_on for low speed region is less than that for high speed region, i.e., V_on depends on v_D rather than v_S. A similar explanation is valid for $i_a<0$. On the other hand, since on-voltages of both diode and IGBT vary with the RMS value of phase current, average on-voltage V_on varies with load even though rotor speed is maintained. In addition, turn off time also varies with operating point due to parasitic capacitors [5]. Accordingly, on-voltages and turn-off time listed in Table I are not always valid. In other words, DTCT varies with operating point. Since it is difficult to measure those parameters individually at various operating points, DTCT is identified online in this paper.

IV. ONLINE IDENTIFICATION OF DTCT

A. d-q Axes DTCV

Fig. 6 shows the numerical results of DTCV for inverter fed PMSM drive. In these numerical results, the rotor speed of PMSM is 1500 r/min (driving frequency is 50 Hz). The

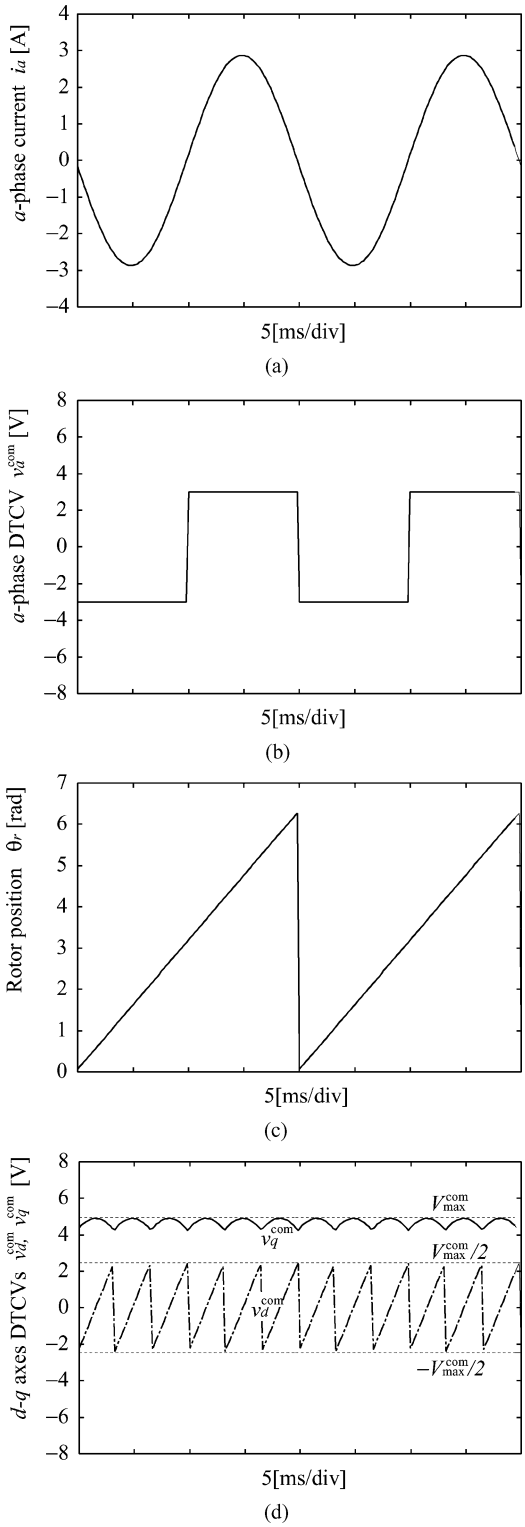

Fig. 6. Numerical result of DTCV when d-axis current is zero [50 Hz (1500 r/min), 2.0 A]. (a) a-phase current. (b) a-phase DTCV. (c) Electrical angle of rotor position. (d) d-q axes DTCVs.

d-axis current i_d is set at zero. The desired DTCT T_c, switching period T_s, and dc-link voltage V_dc are set at 3, 200 μs, and 200 V, respectively. Fig. 6(a) shows a-phase current i_a. Since the polarity of phase DTCV depends on that of phase current,

TABLE II
THEORETICAL d-q AXES DTCVS FOR $i_d = 0$

θ_r	v_d^{com}	v_q^{com}
$0<\theta_r\leq\frac{\pi}{3}$	$-V_{\max}^{\mathrm{com}}\cos(\theta_r+\frac{\pi}{3})$	$V_{\max}^{\mathrm{com}}\sin(\theta_r+\frac{\pi}{3})$
$\frac{\pi}{3}<\theta_r\leq\frac{2}{3}\pi$	$-V_{\max}^{\mathrm{com}}\cos\theta_r$	$V_{\max}^{\mathrm{com}}\sin\theta_r$
$\frac{2}{3}\pi<\theta_r\leq\pi$	$-V_{\max}^{\mathrm{com}}\cos(\theta_r-\frac{\pi}{3})$	$V_{\max}^{\mathrm{com}}\sin(\theta_r-\frac{\pi}{3})$
$\pi<\theta_r\leq\frac{4}{3}\pi$	$V_{\max}^{\mathrm{com}}\cos(\theta_r+\frac{\pi}{3})$	$-V_{\max}^{\mathrm{com}}\sin(\theta_r+\frac{\pi}{3})$
$\frac{4}{3}\pi<\theta_r\leq\frac{5}{3}\pi$	$V_{\max}^{\mathrm{com}}\cos\theta_r$	$-V_{\max}^{\mathrm{com}}\sin\theta_r$
$\frac{5}{3}\pi<\theta_r\leq 2\pi$	$V_{\max}^{\mathrm{com}}\cos(\theta_r-\frac{\pi}{3})$	$-V_{\max}^{\mathrm{com}}\sin(\theta_r-\frac{\pi}{3})$

a-phase DTCV v_a^{com} is determined from (1) as shown in Fig. 6(b). Although waveforms of b-phase and c-phase DTCVs are not shown in this figure, they are also determined in a similar way. Fig. 6(c) shows electrical angle of rotor position θ_r of PMSM. Here, zero point of rotor position corresponds to zero instant of a-phase current i_a because d-axis current is equal to zero. Phase DTCVs formulated such as (1) are transformed into d-q axes DTCVs using the transformation matrix given as

$$\boldsymbol{C} = \sqrt{\frac{2}{3}}\begin{bmatrix} \cos\theta_\mathrm{r} & \cos\left(\theta_\mathrm{r}-\frac{2}{3}\pi\right) & \cos\left(\theta_\mathrm{r}+\frac{2}{3}\pi\right) \\ -\sin\theta_\mathrm{r} & -\sin\left(\theta_\mathrm{r}-\frac{2}{3}\pi\right) & -\sin\left(\theta_\mathrm{r}+\frac{2}{3}\pi\right) \end{bmatrix}. \tag{4}$$

As shown in Fig. 6(d), q-axis DTCV v_q^{com} is a dc voltage with pulsation. The maximum value of q-axis DTCV is given as

$$V_{\max}^{\mathrm{com}} = 2\sqrt{\frac{2}{3}}\frac{T_c}{T_\mathrm{s}}V_\mathrm{dc}. \tag{5}$$

It is noted that maximum value $V_{\max}^{\mathrm{com}}$ is proportional to DTCT T_c as long as both switching period T_s and dc-link voltage V_dc are constants. In other words, $V_{\max}^{\mathrm{com}}$ varies with T_c. On the other hand, d-axis DTCV v_d^{com} is an ac voltage. Its amplitude corresponds to $V_{\max}^{\mathrm{com}}/2$. The d-q axes DTCVs vary every $\pi/3$ rad on rotor position, i.e., fundamental frequency of d-q axes DTCVs is six times of driving frequency.

Table II summarizes theoretical d-q axes DTCVs for rotor position for $i_d = 0$. Average q-axis DTCV over $\pi/3$ rad is derived from Table II as

$$V_{\mathrm{ave}}^{\mathrm{com}} = \frac{3}{\pi}V_{\max}^{\mathrm{com}}\int_0^{\pi/3}\sin\left(\theta_\mathrm{r}+\frac{\pi}{3}\right)d\theta_\mathrm{r} = \frac{3}{\pi}V_{\max}^{\mathrm{com}}. \tag{6}$$

DTCT T_c is identified based on the information of average q-axis DTCV.

B. Identification of DTCT

Phase DTCV corresponds to the average value of the difference between ideal and actual inverter output voltages over switching period. It is important for dead-time compensation strategy to determine DTCV adequately. As can be seen from (1), the amplitude of phase DTCV is proportional to DTCT T_c as long as both switching period T_s and dc-link voltage V_dc are constants. DTCT is usually an unknown parameter. Furthermore, DTCT varies with operating point as indicated in Section III. Then, DTCT is identified online.

Rearranging (5) gives the analytical equation of DTCT as

$$T_c = \frac{\sqrt{6}}{4}\frac{V_{\max}^{\mathrm{com}}}{V_{\mathrm{dc}}}T_{\mathrm{s}}. \tag{7}$$

Since dc-link voltage V_{dc} and switching period T_{s} are known parameters, only the maximum q-axis DTCV $V_{\max}^{\mathrm{com}}$ is estimated for the sake of calculation of DTCT. DTCT is identified by the following procedure. It is assumed that undesirable characteristics of inverter yield d-q axes disturbance voltages (v_d^{dt}, v_q^{dt}) in current control loop on the vector-controlled PMSM drive system. Since q-axis disturbance voltage v_q^{dt} to be compensated corresponds to q-axis DTCV v_q^{com}, its maximum value is regarded as $V_{\max}^{\mathrm{com}}$. A disturbance observer estimates q-axis disturbance voltage v_q^{dt}. The maximum value of estimated q-axis disturbance voltage is regarded as $\hat{V}_{\max}^{\mathrm{com}}$. However, it is difficult to detect the reliable maximum value of q-axis disturbance voltage when estimated q-axis voltage is unsettled. In order to overcome this problem, DTCT is identified based on average q-axis DTCV $V_{\mathrm{ave}}^{\mathrm{com}}$ instead of maximum q-axis DTCV $V_{\max}^{\mathrm{com}}$. The relationship between DTCT T_c and average q-axis DTCV $V_{\mathrm{ave}}^{\mathrm{com}}$ is derived from (6) and (7) as

$$T_c = \frac{\pi}{3}\frac{\sqrt{6}}{4}\frac{V_{\mathrm{ave}}^{\mathrm{com}}}{V_{\mathrm{dc}}}T_{\mathrm{s}}. \tag{8}$$

Regarding the average value of estimated q-axis disturbance voltage as $\hat{V}_{\mathrm{ave}}^{\mathrm{com}}$ gives the identification equation of DTCT as

$$\hat{T}_c = \frac{\pi}{3}\frac{\sqrt{6}}{4}\frac{\hat{V}_{\mathrm{ave}}^{\mathrm{com}}}{V_{\mathrm{dc}}}T_{\mathrm{s}}. \tag{9}$$

As can be seen from Table II, $V_{\max}^{\mathrm{com}}$ can be estimated using d-axis disturbance voltage because it is also related to d-axis DTCV v_d^{com}. However, the maximum value of estimated d-axis disturbance voltage in high speed region does not agree with that of d-axis DTCV any longer because the fundamental frequency of d-axis disturbance voltage exceeds the bandwidth of disturbance observer. In addition, since the average value of d-axis DTCV is theoretically equal to zero, the average value of estimated d-axis voltage has no use for identification of DTCT. In contrast, (9) hardly suffers from increase of driving frequency because q-axis disturbance voltage is a dc voltage and its average value is utilized for calculation of DTCT. For above reasons, DTCT is calculated using q-axis disturbance voltage.

C. Estimation of q-Axis Disturbance Voltage

This paper focuses on dead time compensation for the vector-controlled PMSM. Disturbance observer for q-axis disturbance voltage is derived from the voltage equation of PMSM in the rotor reference frame. The voltage equation is given as

$$\left.\begin{aligned} v_d &= Ri_d + Lpi_d + v_{dd} \\ v_q &= Ri_q + Lpi_q + v_{qd} \end{aligned}\right\} \tag{10}$$

where R, L, and p are armature resistance, armature inductance, and differential operator, respectively. Decoupling voltages are defined as

$$\left.\begin{aligned} v_{dd} &= -\omega_{\mathrm{r}} L i_q \\ v_{qd} &= \omega_{\mathrm{r}}(Li_d + K_{\mathrm{e}}) \end{aligned}\right\} \tag{11}$$

where ω_{r} and K_{e} are electrical angular velocity and electromotive force (emf) constant, respectively.

The commanded voltage generated with current controller without dead time compensation strategy increases by disturbance voltages (v_d^{dt}, v_q^{dt}) to reduce current error against the disturbance voltage. The voltage equation for current control loop is expressed as

$$\left.\begin{aligned} v_d^* &= Ri_d + Lpi_d + v_{dd} + v_d^{dt} \\ v_q^* &= Ri_q + Lpi_q + v_{qd} + v_q^{dt} \end{aligned}\right\} \tag{12}$$

where superscript "$*$" denotes commanded value. As a result, commanded voltage disagrees with actual one, i.e., (12) disagrees with (10).

In contrast, the voltage equation for current control loop with the dead time compensation strategy is given as

$$\left.\begin{aligned} v_d^* + v_d^{\mathrm{com}} &= Ri_d + Lpi_d + v_{dd} + v_d^{dt} \\ v_q^* + v_q^{\mathrm{com}} &= Ri_q + Lpi_q + v_{qd} + v_q^{dt} \end{aligned}\right\}. \tag{13}$$

As can be seen from (13), commanded voltages (v_d^*, v_q^*) correspond to actual one (v_d, v_q) provided that d-q axes DTCVs $(v_d^{\mathrm{com}}, v_q^{\mathrm{com}})$ agree with d-q axes disturbance voltages (v_d^{dt}, v_q^{dt}).

In this paper, only q-axis disturbance observer is developed because q-axis disturbance voltage is utilized for identification of DTCT. Assuming that q-axis disturbance voltage seldom changes during control period, i.e., $\dot{v}_q^{dt} = 0$, the state equation and output equation of PMSM taking disturbance voltage into account are expressed as

$$\begin{aligned} \dot{\boldsymbol{x}} &= \frac{d}{dt}\begin{bmatrix} i_q \\ v_q^{dt} \end{bmatrix} \\ &= \begin{bmatrix} -\frac{R}{L} & -\frac{1}{L} \\ 0 & 0 \end{bmatrix}\begin{bmatrix} i_q \\ v_q^{dt} \end{bmatrix} + \begin{bmatrix} \frac{1}{L} \\ 0 \end{bmatrix}(v_q' - v_{qd}) \end{aligned} \tag{14}$$

$$\boldsymbol{y} = [\,1 \quad 0\,]\begin{bmatrix} i_q \\ v_q^{dt} \end{bmatrix} \tag{15}$$

where $v_q' = v_q^* + v_q^{\mathrm{com}}$, $\boldsymbol{x}$ and $\boldsymbol{y}$ are state vector and output vector, respectively. From (14) and (15), disturbance observer is derived as

$$\begin{aligned} \dot{\hat{\boldsymbol{x}}} = \frac{d}{dt}\begin{bmatrix} \hat{i}_q \\ \hat{v}_q^{dt} \end{bmatrix} &= \begin{bmatrix} -G_1 - \frac{R}{L} & -\frac{1}{L} \\ -G_2 & 0 \end{bmatrix}\begin{bmatrix} \hat{i}_q \\ \hat{v}_q^{dt} \end{bmatrix} \\ &\quad + \begin{bmatrix} G_1 \\ G_2 \end{bmatrix} i_q + \begin{bmatrix} \frac{1}{L} \\ 0 \end{bmatrix}(v_q' - v_{qd}) \end{aligned} \tag{16}$$

where $G_1 = -(R/L + \gamma_1 + \gamma_2)$, $G_2 = -L\gamma_1\gamma_2$, γ_1 and γ_2 are observer poles.

The part framed by dashed line in Fig. 2 is the proposed dead-time compensator. Disturbance observer estimates q-axis disturbance voltage v_q^{dt} with the use of q-axis current i_q and q-axis voltage v_q'. Then, estimated q-axis disturbance voltage is averaged by the following procedure illustrated in Fig. 7.

1) Estimated q-axis disturbance voltage $\hat{v}_q^{dt}$ is integrated during the interval from t_k to t_{k+n_1}. Here, sampling points t_k and t_{k+n_1} mean first and second zero cross points of a-phase current i_a, respectively.

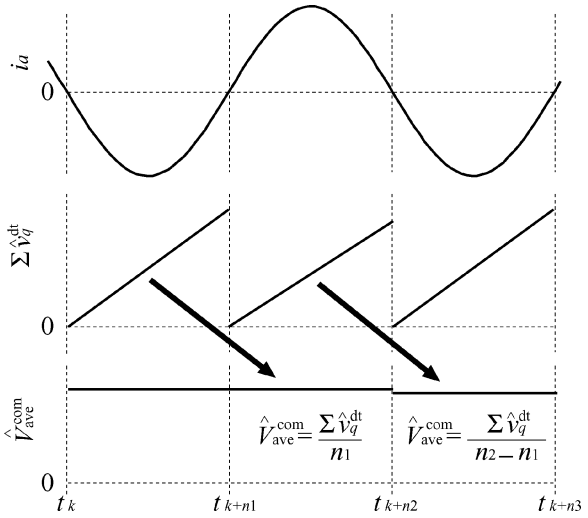

Fig. 7. Average method for q-axis disturbance voltage.

TABLE III
SPECIFICATIONS OF TESTED PMSM

rated power	P_n	160 W
rated torque	τ_n	0.5 N·m
maximum rated speed	N_n	3000 r/min
armature resistance	R	2.20 Ω
armature inductance	L	0.0065 H
emf constant	K_e	0.0658 V·s/rad
number of pole-pairs	P	2

2) At sampling point t_{k+n_1}, integrated q-axis disturbance voltage is averaged as

$$V_{\text{ave}}^{\text{com}} = \frac{\sum \hat{v}_q^{dt}}{n_1}. \tag{17}$$

3) Average value $V_{\text{ave}}^{\text{com}}$ is utilized for identification of DTCT during the interval from t_{k+n_1} to t_{k+n_2}.
4) $V_{\text{ave}}^{\text{com}}$ is updated at sampling point t_{k+n_2} and utilized during the interval from t_{k+n_2} to t_{k+n_3}, sequentially.

DTCT T_c is calculated from (9) using estimated average q-axis disturbance voltage $\hat{V}_{\text{ave}}^{\text{com}}$. Then, a-phase DTCV v_a^{com} is calculated from (1). Similarly, b-phase and c-phase DTCVs $(v_b^{\text{com}}, v_c^{\text{com}})$ are also calculated. After these DTCVs are added to commanded voltages (v_a^*, v_b^*, v_c^*), corrected voltages (v_a', v_b', v_c') are utilized for PWM inverter.

V. SIMULATION AND EXPERIMENTAL RESULTS

Table III shows the specifications of tested PMSM employed in simulation and experiment. Two PI controllers are utilized for speed controller (SC) and current controller (CC) in the vector-controlled PMSM drive system indicated in Fig. 2. Control parameters are shown in Table IV. The pole of observer has been selected carefully because it affects the performance of disturbance observer. In this case, the actual value of q-axis disturbance voltage cannot be obtained, while the actual value of q-axis current can be obtained. For this reason, the poles of observer are selected based on the accuracy of estimated q-axis current. Fig. 8 shows the estimation results of q-axis current for various poles $\gamma = \gamma_1 = \gamma_2$. For $\gamma = -1000$, estimation is poor, i.e., estimated current pulsates. For $\gamma = -2000$, q-axis current is estimated without serious delay. For $\gamma = -3000$, q-axis current is estimated well, that is, high-frequency components are also estimated. However, high-frequency components are not required in the proposed method because estimated q-axis disturbance voltage is averaged. For system stability point of view, the pole of observer has been conservatively selected at -2000.

Fig. 9 shows the simulation result for the proposed dead-time compensation strategy. The rotor speed of PMSM is 300 r/min (driving frequency is 10 Hz). The load torque is 0.18 N·m (36.5% of the rated torque). The d-axis current i_d is controlled at zero. In this simulation, the desired DTCT T_c is set at 3μs. Fig. 9(a) shows q-axis disturbance voltage v_q^{dt} estimated by disturbance observer. Although estimated q-axis disturbance voltage (solid line) practically agrees with ideal q-axis DTCV (dashed line), the maximum value of estimated q-axis disturbance voltage is extremely greater than that of ideal q-axis DTCV in some

TABLE IV
CONTROL PARAMETERS

dc-link voltage	V_{dc}	200 V
carrier frequency	f_c	5 kHz
switching period	T_s	200 μs
control period	T_{ctl}	200 μs
proportional gain for SC	K_{ps}	0.01
integral gain for SC	K_{is}	0.30
proportional gain for CC	K_{pc}	10
integral gain for CC	K_{ic}	1000
poles of observer	γ_1, γ_2	-2000

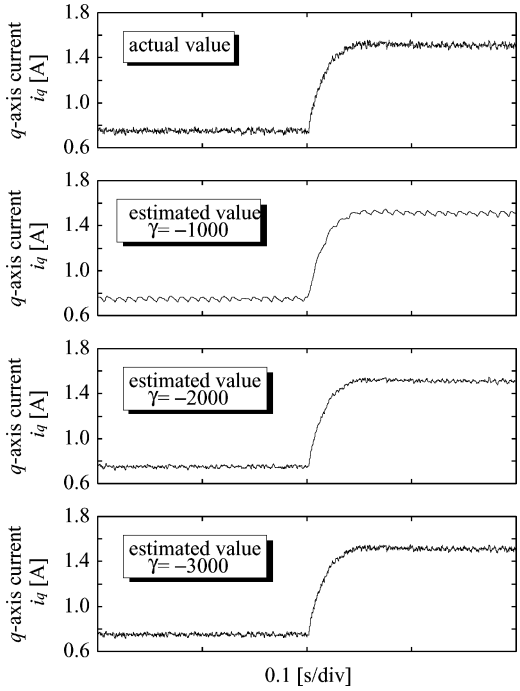

Fig. 8. Simulation results of estimation of q-axis current for various poles of observer.

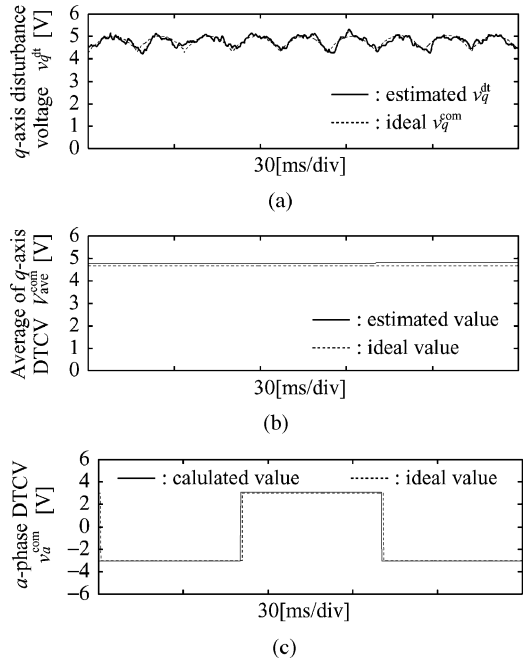

Fig. 9. Simulation results for estimation of DTCV [10 Hz (300 r/min), 0.8 A]. (a) q-axis disturbance voltage. (b) Average q-axis DTCV. (c) a-phase DTCV.

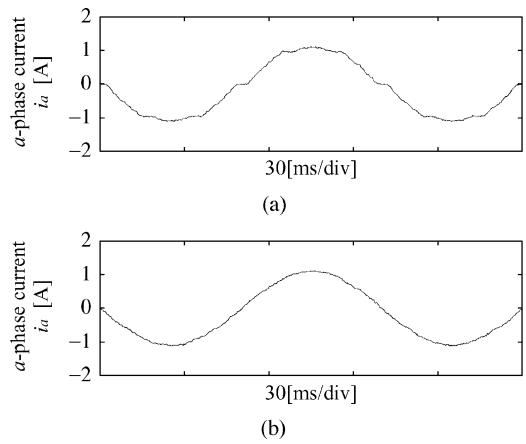

Fig. 10. Simulation results for comparison of a-phase current (a) without (b) with the dead time compensation strategy [10 Hz (300 r/min), 0.8 A].

instants. An extreme value results in improper estimation of the maximum value of q-axis disturbance voltage. As a result, DTCT is improperly identified. To overcome this problem, the average value of estimated q-axis disturbance voltage is utilized for identification of DTCT. Fig. 9(b) shows q-axis disturbance voltage averaged by the method illustrated in Fig. 7. As can be confirmed from Fig. 9(b), there is not prominent error between the average values of q-axis disturbance voltage and ideal q-axis DTCV. Fig. 9(c) shows a-phase DTCV $v_a^{\rm com}$. The amplitude of DTCV (solid line) almost agrees with that of the ideal DTCV (dashed line).

Fig. 10 shows a-phase current i_a with/without dead time compensation strategy. Distortion of phase current is suppressed by applying the proposed dead time compensation strategy.

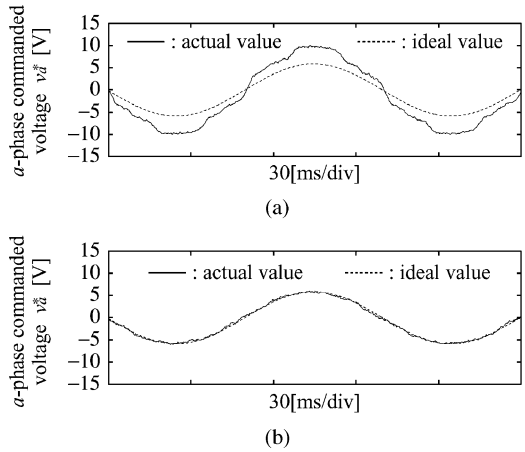

Fig. 11. Simulation results for comparison of a-phase commanded voltage (a) without (b) with the dead time compensation strategy [10 Hz (300 r/min), 0.8 A].

Fig. 11 shows a-phase commanded voltage v_a^* with/without the proposed dead time compensation strategy. In order to confirm that commanded voltage quantitatively agrees with fundamental phase voltage of inverter, the commanded voltage is compared with output voltage when we use an ideal power source (sinusoidal source). Commanded voltage without dead-time compensation strategy disagrees with ideal output voltage because the commanded voltage is adjusted so as to reduce current error against disturbance voltage due to undesirable characteristics of inverter in feedback current control loop. Although the effect of disturbance voltage is somewhat suppressed by applying feedback current control, the waveform of commanded voltage v_a^* is not sinusoidal any longer. In contrast, commanded voltage with the proposed dead-time compensation strategy almost agrees with ideal output voltage. In other words, since the proposed dead time compensator performs well, it is not necessary that current controller reacts against disturbance voltage. As a result, waveform of commanded voltage v_a^* is sinusoidal.

Fig. 12 shows the experimental results for the proposed dead-time compensation strategy illustrated in Fig. 2. Most of the parts of the system shown in Fig. 2 are implemented in a DSP TMS320C32. The operating conditions are same as the simulation. Fig. 12(a) shows the estimation result of q-axis disturbance voltage. It is confirmed from this figure that estimated q-axis disturbance voltage is dc voltage with pulsation. The fundamental frequency of this pulsation is six times of driving frequency as ideal q-axis DTCV. Estimated q-axis disturbance voltage is averaged as shown in Fig. 12(b). DTCT is calculated from (9) using estimated average q-axis DTCV. Then, the amplitude of a-phase DTCV is decided as shown in Fig. 12(c).

As can be seen from Fig. 13, distortion of a-phase current is suppressed by applying the proposed dead-time compensation strategy. The a-phase commanded voltage for the proposed dead time compensation strategy is compared with commanded voltage without dead-time compensation strategy in Fig. 14. Although this experimental result resembles the simulation result shown in Fig. 11, quantitative evaluations are impossible from this figure because the fundamental output voltage of inverter

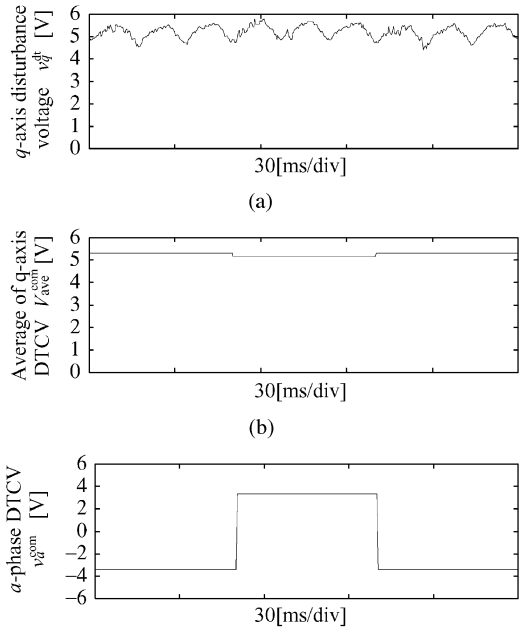

Fig. 12. Experimental results for estimation of DTCV [10 Hz (300 r/min), 0.8 A]. (a) q-axis disturbance voltage. (b) Average q-axis DTCV. (c) a-phase DTCV.

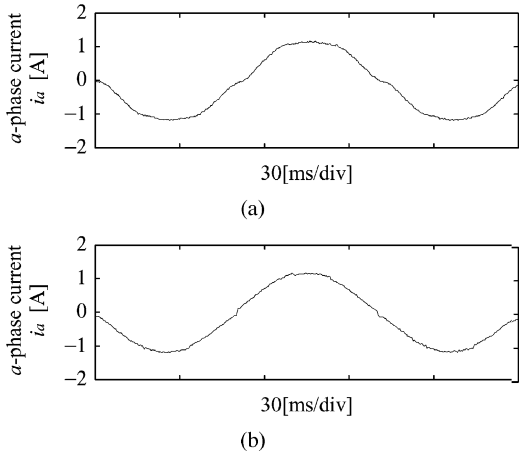

Fig. 13. Experimental results for comparison of a-phase current (a) without (b) with the proposed dead time compensation strategy [10 Hz (300 r/min), 0.8 A].

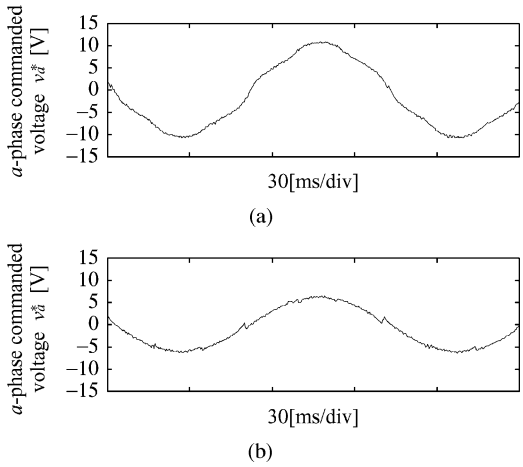

Fig. 14. Experimental results for comparison of a-phase commanded voltage (a) without (b) with the proposed dead time compensation strategy. [10 Hz (300 r/min), 0.8 A].

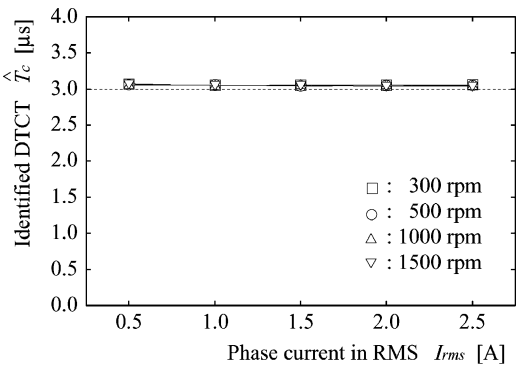

Fig. 15. Simulation result for the identification of DTCT at various operating points.

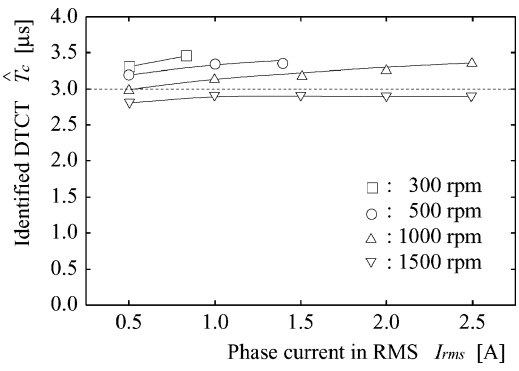

Fig. 16. Experimental result for the identification of DTCT at various operating points.

is not available in this experiment. In order to evaluate performance of the proposed dead-time compensation strategy, commanded voltage is utilized for calculation of active power and the calculated active power is compared with measured active power. The detail of this result is discussed at the end of this section.

Fig. 15 shows the simulation result for the identification of DTCTs at various operating points. In this simulation, the desired DTCT is set at 3μs. DTCT can be identified within range of 3.0% (average error is 1.8%) regardless of operating point. Identified DTCT tends to be slightly greater than desired DTCT because averaging of estimated q-axis disturbance voltage cannot perfectly clear off extreme values. Nevertheless, it is acceptable error range in this system.

Fig. 16 shows the experimental results for the identification of DTCTs at various operating points. In our experimental setup, a generator coupled with tested PMSM is utilized as load system. Load torque for low speed region is limited due to low output power of the generator. As expected earlier, identified DTCT tends to increase with decreasing rotor speed. On the other

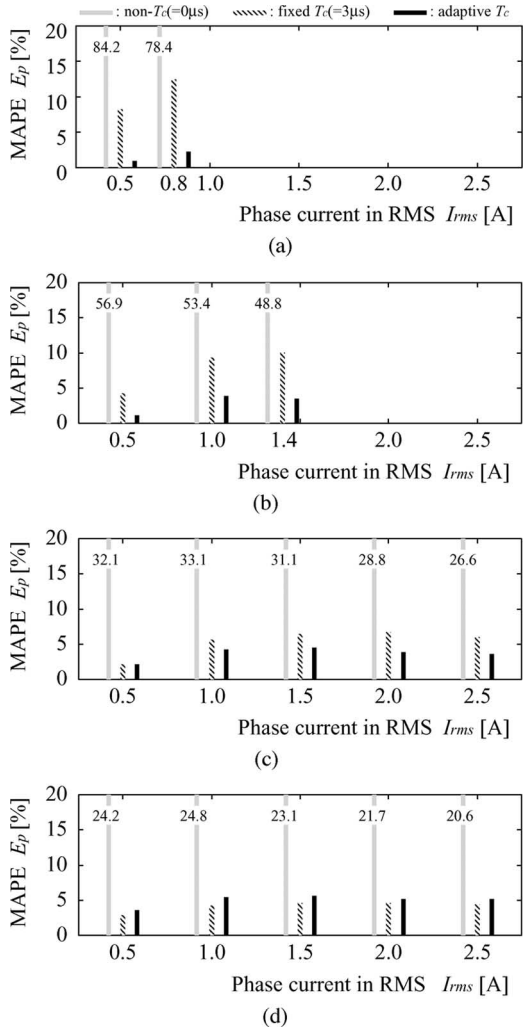

Fig. 17. Comparison between calculated and measured active power for various operating points: (a) 300 r/min, (b) 500 r/min, (c) 1000 r/min, and (d) 1500 r/min.

hand, identified DTCT increases with the RMS value of phase current.

In order to evaluate the proposed dead-time compensation strategy quantitatively, the active power calculated with the use of commanded voltage is compared with the active power measured with the help of digital power meter WT230. The calculated active power is obtained from

$$P_{\rm in}^{\rm c} = v_d^* i_d + v_q^* i_q \tag{18}$$

where v_d^* and v_q^* are d-q axes commanded voltages and i_d and i_q are the d-q axes currents.

Fig. 17 shows the MAPE of calculated active power for various DTCT conditions. MAPE is defined as

$$E_p = \frac{1}{N}\sum_{n=1}^{N}\left(\frac{|P_{\rm in}^{\rm c} - P_{\rm in}^{\rm m}|}{P_{\rm in}^{\rm m}}\right) \times 100 \tag{19}$$

where $P_{\rm in}^{\rm c}$, $P_{\rm in}^{\rm m}$, and N denote calculated active power, measured active power, and numbers of data, respectively. In order to confirm the validity of the proposed method, MAPE for adaptive DTCT is compared with that for both non-DTCT ($T_c = 0$ μs) and fixed DTCT ($T_c = 3$ μs).

MAPE for non-DTCT is the largest for any operating point. It is noted that the value of MAPE for non-DTCT is inscribed in this figure because it exceeds the scale of vertical axis. Comparison between adaptive DTCT and fixed DTCT offers the following remarks.

1) MAPE for adaptive DTCT is generally less than that for fixed DTCT.
2) Remarkable differences of MAPE appears at the operating point in which identified DTCT deviates from 3 μs. For example, MAPE for adaptive DTCT is much less than that for fixed DTCT at operating point (300 r/min, 0.8 A). On the other hand, MAPE for adaptive DTCT is almost same as MAPE for fixed DTCT at 1500 r/min because identified DTCT at this operating point is close to 3 μs.

The fact that MAPE for adaptive DTCT is within 5% confirms the validity of the proposed dead time compensation strategy.

VI. Conclusion

This paper has proposed the adaptive dead-time compensation strategy for typical vector-controlled PMSM drive in which d-axis current is set at zero. In the first phase, it has been pointed out that the DTCT that includes dead time, turn on/off time of switching devices, and on-voltage components of switching devices and diodes varies with operating point. In the second phase, the relationship between DTCT and q-axis DTCV in the rotor reference frame has been analyzed and the analytical equation of DTCT has been derived. DTCT is identified online with the use of estimated q-axis disturbance voltage in current control loop in the vector-controlled PMSM drive system with the assumption that q-axis DTCV corresponds to q-axis disturbance voltage to be compensated. Identified DTCT is adaptively utilized for the dead time compensation strategy. In order to confirm the validity of the proposed dead time compensation strategy, simulation and experimental results have been performed. Commanded voltage with the proposed dead time compensation strategy agrees with ideal output voltage in the simulation. The active power calculated with the use of commanded voltage agrees with the active power measured with digital power meter within 5% MAPE in experimentation. Furthermore, MAPE for adaptive DTCT is much less than that for fixed DTCT in low-speed region. The accuracy of the armature resistance is also required to obtain fundamental phase voltage. The next research goal is to compensate the effect of armature resistance variation in low-speed region.

References

[1] J.-S. Lee, T. Takeshita, and N. Matsui, "Stator-flux-oriented sensorless induction motor drive for optimum low-speed performance," *IEEE Trans. Ind. Appl.*, vol. 33, no. 5, pp. 1170–1176, Sep. 1997.

[2] J. Holtz and J. Quan, "Sensorless vector control of induction motors at very low speed using a nonlinear inverter model and parameter identification," *IEEE Trans. Ind. Appl.*, vol. 38, no. 4, pp. 1087–1095, July 2002.

[3] S.-G. Jeong and M.-H. Park, "The analysis and compensation of dead time effects in PWM inverters," *IEEE Trans. Ind. Electron.*, vol. 38, no. 2, pp. 108–114, Apr. 1991.

[4] J.-W. Choi and S.-K. Sul, "Inverter output voltage synthesis using novel dead time compensation," *IEEE Trans. Power Electron.*, vol. 11, no. 2, pp. 221–227, Mar. 1996.
[5] R. J. Kerkman, D. Leggate, D. W. Schlegel, and C. Winterhalter, "Effects of parasitics on the control of voltage source inverter," *IEEE Trans. Power Electron.*, vol. 18, no. 1, pp. 140–150, Jan. 2003.
[6] H.-S. Kim, H.-T. Moon, and M.-J. Youn, "On-line dead time compensation method using disturbance observer," *IEEE Trans. Power. Electron.*, vol. 18, no. 6, pp. 1336–1345, Nov. 2003.

Naomitsu Urasaki (M'98) was born in Okinawa, Japan, in 1973. He received the B.S., M.S., and Ph.D. degrees from the University of the Ryukyus, Okinawa, in 1996, 1998, and 2004, respectively, all in electrical engineering.

Since 1998, he has been with the Department of Electrical and Electronics Engineering, Faculty of Engineering, University of the Ryukyus, where he is currently working as a Research Associate. His research interests include the areas of ac motor drives.

Dr. Urasaki is a member of the Institute of Electrical Engineers of Japan.

Tomonobu Senjyu (A'84–M'02–SM'06) was born in Saga, Japan, in 1963. He received the B.S. and M.S. degrees from the University of the Ryukyus, Okinawa, Japan, in 1986 and 1988, respectively, and the Ph.D. degree from Nagoya University, Aichi, Japan, in 1994, all in electrical engineering.

Since 1988, he has been with the Department of Electrical and Electronics Engineering, Faculty of Engineering, University of the Ryukyus, where he is currently working as a Professor. His research interests include stability of ac machines, advanced control of electrical machines, and power electronics.

Prof. Senjyu is a member of the IET of U.K. and the Institute of Electrical Engineers of Japan. He is also a Chartered Engineer in the U.K.

Katsumi Uezato was born in Okinawa, Japan, in 1940. He received the B.S. degree from the University of the Ryukyus, Okinawa, Japan, in 1963, the M.S. degree from Kagoshima University, Kagoshima, Japan, in 1972, and the Ph.D. degree form Nagoya University, Nagoya, Japan, in 1983, all in electrical engineering.

Since 1972, he has been with the Department of Electrical and Electronics Engineering, Faculty of Engineering, University of the Ryukyus, where he has been engaged in research on stability and control of synchronous machines.

Dr. Uezato is a member of the Institute of Electrical Engineers of Japan.

Toshihisa Funabashi (M'90–SM'96) was born in Aichi, Japan, in 1951. He received the B.S. degree from Nagoya University, Aichi, Japan, in 1975, and the Ph.D. degree from Doshisha University, Kyoto, Japan, in 2000, both in electrical engineering.

In 1975, he joined Meidensha Corporation, Tokyo, Japan, where he was engaged in research on power system analysis. Currently, he is working as a Senior Engineer at the Power System Engineering Division, Meidensha Corporation.

Dr. Funabashi is a member of the IET of U.K. and the Institute of Electrical Engineers of Japan. He is also a Chartered Engineer in the U.K.